Adsorption of CO_2, CH_4, CO_2/N_2 and CO_2/CH_4 in Novel Activated Carbon Beads: Preparation, Measurements and Simulation

Xiaohong Shao
College of Science, Beijing University of Chemical Technology, Beijing 100029, China

Key Laboratory for Nanomaterials, Ministry of Education, Beijing University of Chemical Technology, Beijing 100029, China

Zhenhe Feng
College of Science, Beijing University of Chemical Technology, Beijing 100029, China

Ruisheng Xue
Key Laboratory of Carbon Fiber and Functional Polymers, Ministry of Education, Beijing University of Chemical Technology, Beijing 100029, China

Congcong Ma and Wenchuan Wang
Key Laboratory for Nanomaterials, Ministry of Education, Beijing University of Chemical Technology, Beijing 100029, China

Xuan Peng
College of Information Science, Beijing University of Chemical Technology, Beijing 100029, China

Dapeng Cao
Key Laboratory for Nanomaterials, Ministry of Education, Beijing University of Chemical Technology, Beijing 100029, China

DOI 10.1002/aic.12515
Published online February 15, 2011 in Wiley Online Library (wileyonlinelibrary.com).

A series of high performance carbonaceous mesoporous materials: activated carbon beads (ACBs), have been prepared in this work. Among the samples, ACB-5 possesses the BET specific surface area of 3537 $m^2\ g^{-1}$ and ACB-2 has the pore volume of 3.18 $cm^3\ g^{-1}$. Experimental measurements were carried out on the intelligent gravimetric analyzer (IGA-003, Hiden). Carbon dioxide adsorption capacity of 909 mg g^{-1} has been achieved in ACB-5 at 298 K and 18 bar, which is superior to the existing carbonaceous porous materials and comparable to metal-organic framework (MOF)-177 (1232 mg g^{-1}, at 298 K and 20 bar) and covalent-organic framework (COF)-102 (1050 mg g^{-1} at 298 K and 20 bar) reported in the literature. Moreover, methane uptake reaches 15.23 wt % in ACB-5 at 298 K and 18 bar, which is better than MOF-5. To predict the performances of the samples ACB-2 and ACB-5 at high pressures, modeling of the samples and grand canonical Monte Carlo simulation have been conducted, as is presented in our previous work. The adsorption isotherms of CO_2/N_2 and

Correspondence concerning this article should be addressed to W. Wang at wangwc@mail.buct.edu.cn and D. Cao at caodp@mail.buct.edu.cn.

CO_2/CH_4 in our samples ACB-2 and 5 have been measured at 298 and 348 K and different compositions, corresponding to the pre- and postcombustion conditions for CO_2 capture. The Dual-Site Langmuir-Freundlich (DSLF) model-based ideal-adsorbed solution theory (IAST) was also used to solve the selectivity of CO_2 over N_2 and CH_4. The selectivities of ACBs for CO_2/CH_4 are in the range of 2–2.5, while they remain in the range of 6.0–8.0 for CO_2/N_2 at T = 298 K. In summary, this work presents a new type of adsorbent-ACBs, which are not only good candidates for CO_2 and CH_4 storage but also for the capture of carbon dioxide in pre- and postcombustion processes. © 2011 American Institute of Chemical Engineers *AIChE J,* 57: 3042–3051, 2011
Keywords: absorption, materials, simulation, molecular, environmental engineering

Introduction

Emission of carbon dioxide contributes to global warming significantly, which has become a pressing environmental topic now.[1,2] New technologies are therefore required to reduce CO_2 emission to ease climate change. Adsorption via porous materials to remove CO_2 has been developed recently for its economic and environmental advantages.[3] Accordingly, carbonaceous materials,[4–6] zeolites,[7] metal-organic frameworks (MOFs),[8] covalent-organic frameworks (COFs),[9] and zeolitic imidazolate frameworks (ZIFs)[10] are being considered as candidates to capture CO_2.

Moreover, as a major component of natural gas (NG), methane has already been widely studied and applied in many aspects, including in vehicles.[11–13] The reason is that NG is cheaper than conventional petroleum-based gasoline and environment benign due to its clean burning,[14] in particular. Compared with the compressed natural gas (CNG), adsorbed natural gas (ANG) on a suitable microporous adsorbent offers a promising opportunity. Hence, methane adsorption storage has attracted considerable interest for researchers. The adsorption capacity of 35 wt % or 180 V/V at 35 bar at room temperature set by DOE of US is required for ANG, which can compete against the energy density of CNG at 250 bar. Consequently, adsorption storage of methane is also a hot topic in the energy field.

In addition, the separation of CO_2 from mixtures such as flue gas (postcombustion) and NG (precombustion) is very important. NG is mainly composed of methane, carbon dioxide, nitrogen and heavier hydrocarbons. The existence of CO_2 reduces its conversion rate and energy content. On the other hand, nitrogen exists in the flue gas as a major component. Consequently, increasing attention is paid to the separation of CO_2/CH_4 for NG and CO_2/N_2 for flue gas.

It is noticed that among many porous adsorbents, carbonaceous materials with good thermal-stability and low cost have been considered as promising candidates for storage and separation of CO_2. To tackle the tasks mentioned above, the preparation of the carbonaceous materials with high specific surface area (SSA), large pore volume and appropriate pore size is vital to obtain a high uptake and selectivity. Template carbonization has been widely used for the preparation of carbonaceous porous materials in many fields for getting regular pore size in recent years.[15,16] However, the preparation costs, complicated processes, and rather low BET SSA hinder the application of the method. Still, amorphous carbon porous materials can be prepared in an economic way. One of them with a simple preparation process and long history is activated carbon. However, the wide pore size distribution (PSD) and not high enough BET SSA restrict its applications. Consequently, in order to get high BET SSA and appropriate PSD, a new approach is needed for improving carbon activation efficiency.

Motivated by the goals proposed above, in this work, first, a new procedure of carbon bead formation is proposed by mixing coal tar pitches and fumed silica powder together. After activation, adsorption properties of the activated carbon beads (ACBs) are characterized by experiments. Meanwhile, to predict the uptakes of CO_2 and CH_4 at high pressures, the ACB is modeled as slit-like with a PSD, and grand canonical Monte Carlo (GCMC) method simulation is used for the calculation of adsorption isotherms of the ACBs. Then, the isotherms of the mixtures of CO_2/N_2 and CO_2/CH_4 are also measured experimentally for calculations of the selectivities for the ACBs. This article is organized as follows. In "Preparation and Measurements of ACBs" section, the experimental work, including the synthesis, characterization and the gravimetric high-pressure adsorption measurements, is described. The modeling of ACBs and molecular simulation details are depicted in "Modeling of ACB and Molecular Simulation" section. In "Results and Discussion" section, the results obtained by experiment, simulation and modeling are presented. Finally, some conclusions are addressed in "Conclusions" section.

Preparation and Measurements of ACBs

Preparation of ACBs

The selected coal tar pitches (Anshan Steel Co., China) and fumed silica powder (Shandong Yihao Co., China) were mixed at the weight ratio of 4:1. The mixture was then heated at 1 K/min up to 633 K and maintained for 0.5 h at 633 K. Next, the mixture was carbonized at 773 K and 1 bar for 1 h in pure nitrogen. The carbon beads were sifted out by the sieve of 200 meshes. Since it is difficult to get highly porous carbon by physical activation, chemical activation was used here. The carbon beads were mixed with KOH at the KOH/carbon beads weight ratios from 3 to 9. The mixtures were heated up to 1073 K, 1123 K, or 1173 K and were then held for 1 h. After cooling down, the sample was washed with deionized water and dried at 393 K for 12 h in vacuum. Five samples (ACB-x, x = 1–5) with different weight ratios of KOH/carbon beads and different activation temperatures were chosen for adsorption measurements, which are listed in Table 1.

Table 1. Preparation Conditions and Serial Number of ACBs in this Work

Sample	Weight Ratio of KOH/Carbon Beads	Temperature of Activation (°C)
ACB-1	7	900
ACB-2	9	850
ACB-3	9	800
ACB-4	5	900
ACB-5	7	800

Characterization of ACBs

The accelerated surface area and porosimetry apparatus (ASAP 2010, Micromeritics Ins. Corp.) was used for characterization of the samples. In addition, scanning electron microscopy (SEM) images were obtained by means of the Hitachi S-4700 instrument.

Gravimetric high-pressure adsorption measurements

The intelligent gravimetric analyzer (IGA-003, Hiden) was used to measure the adsorption isotherms of CO_2, CH_4, and N_2 and their mixtures for the sample ACBs. Detailed information on the apparatus can be referred to our previous work.[12] To guarantee removal of impurities on micropores, the samples in the vessel of IGA-003 were vacuumed up to 10^{-5} Pa, and out-gassed at 10^{-5} Pa and 573 K for 24 h before the measurements, heated by an inherent furnace. A built-in water bath was used to maintain the adsorption temperatures from 298 to 353 K. To guarantee equilibration, 1.5 h was needed for a data point in the measurements. CO_2 is of the purity of 0.995 (mol), CH_4 is of the purity of 0.999 (mol), and N_2 is of the purity of 0.995(mol) in our experiment, which were produced by Haipu Gas Factory, Beijing, China.

Modeling of ACB and Molecular Simulation

A porous carbon bead is modeled as the slit-shaped carbon layers. The distance between two layers is the lattice distance of 0.335 nm. After activation by KOH, a PSD was generated. Consequently, the ACBs are modeled as porous carbon possessing slit-like pores with a PSD, in accordance with our previous work.[12] Similar modeling works can also be referred to the literature.[17,18]

Table 2. Parameters of Potential Models for Fluids and ACB in GCMC Simulation*

Species	Site	σ/nm	$\varepsilon_{ff}k_B^{-1}$ (K)	q (e)
CO_2	C	0.2789	29.66	+0.576
	O	0.3011	82.96	−0.288
N_2	N	0.332	36.4	0
CH_4	CH_4	0.381	148.1	0

*The parameters for CO_2, N_2, CH_4 are taken from Refs. [20], [21], and [22], respectively. CO_2 is modeled as a combination of the Lennard-Jones (LJ) and Columbic potentials.

Adsorption of carbon dioxide, methane and nitrogen was simulated by using GCMC simulation. The PSD of ACBs was calculated by a combined method of statistical integral equation (SIE) and GCMC by assuming that the carbon pores are slit shaped, as is discussed in the literature.[12,19] CO_2 is represented as a three-site molecule, and the CO_2–CO_2 interaction is modeled as a combination of the Lennard-Jones (LJ) and Columbic potentials, where the bond angle is 180° and the bond length is 0.119 nm.[20] The partial charges on C and O atoms are 0.576 e and −0.288 e, respectively. N_2 molecules are represented as a two-site potential model.[21] CH_4 is modeled as one-site interaction with the LJ model.[22,23] The interaction between the fluid molecule and wall is described by the well-known Steele's 10-4-3 potential model.[24] All the parameters used here are listed in Table 2. For every state, 2×10^7 configurations were generated and the first 1×10^7 configurations were discarded to ensure the equilibration in GCMC simulation. The computational details can be referred to our previous work.[12,19]

Results and Discussion

Structure and porosity analysis

Figure 1 shows SEM images of ACBs in high and low resolution, respectively. From the images of low resolution (in

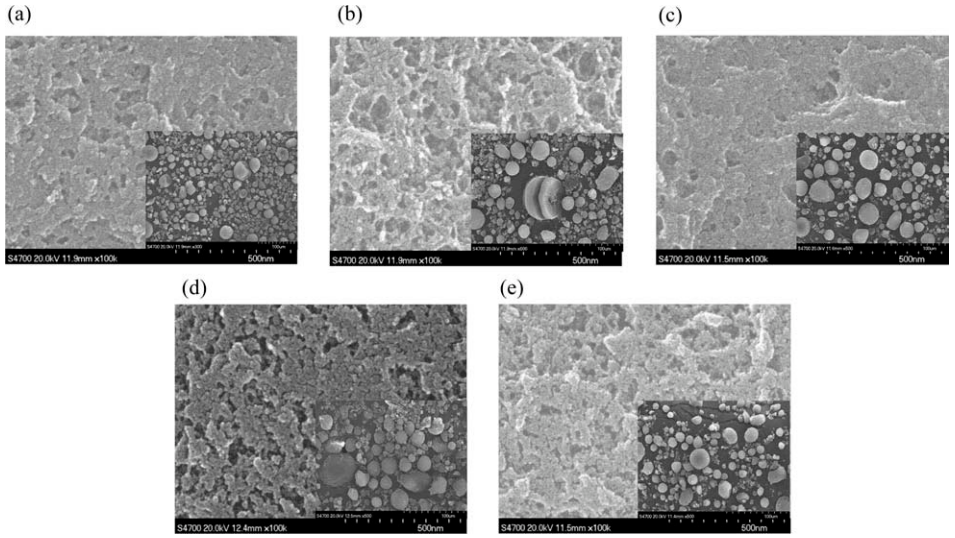

Figure 1. SEM photos of ACBs in high and low magnifications.

(a) ACB-1, (b) ACB-2, (c) ACB-3, (d) ACB-4, (e) ACB-5. The images of low magnification are in the right-bottom corner of Figures 1a–e, respectively.

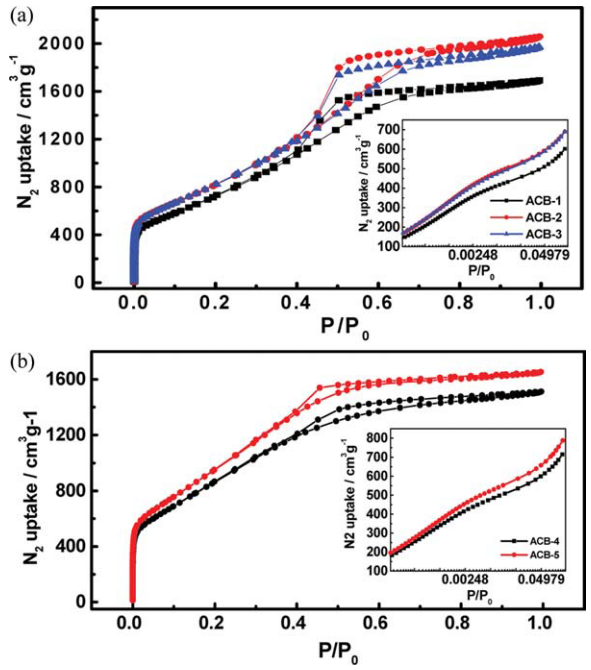

Figure 2. Nitrogen adsorption-desorption isotherms of all the samples measured by ASAP-2010 at 77 K.

The enhanced adsorption-desorption isotherms at low pressures are in the right bottom corner. Figure 2a presents the isotherms of ACB-1, ACB-2, and ACB-3 and Figure 2b shows the isotherms of ACB-4 and ACB-5 [Color figure can be viewed in the online issue, which is available at wileyonlinelibrary.com.]

the right-bottom corner of Figures 1a–e), it is found that most of the beads are sphere shaped. It is also found that SiO_2 is beneficial to the formation of beads. In the activation procedure, KOH reacted with SiO_2. After washing with deionized water, the production of K_2SiO_3 was removed away from the ACBs.[25] The enhancing photo of high resolution shows external pores, which act as channels for fluid molecules passing through. Nitrogen adsorption and desorption isotherms of sample ACB-x (x = 1–5) measured by using ASAP-2010 are shown in Figure 2. Interestingly, ACB-2 sample exhibits a maximum nitrogen adsorption amount, which is more than 2000 $cm^3\ g^{-1}$, higher than the results reported in the literature,[12,26] in which Wang et al.[26] synthesized the activated carbon with N_2 adsorption of more than 1100 $cm^3 g^{-1}$. It is found that the nitrogen uptakes of ACB-2 are the highest, which will be discussed later. In addition, all the isotherms show clear hysteresis loops in a wide relative pressure range of $P/P_0 = 0.35$ to 0.8, where P_0 is the saturated nitrogen vapor pressure at 77 K. According to the IUPAC classifications of pores, these samples reside in the range of mesoporous materials.

The porosity parameters measured in ASAP 2010 are listed in Table 3. The BET SSAs of our samples are in the range of about 2600 to 3500 $m^2\ g^{-1}$. The BET SSA of sample ACB-5 is 3537 $m^2\ g^{-1}$, which is higher than our previous result of a-MCMBs with BET SSA of 3180 $m^2\ g^{-1}$.[12] In addition, the pore volumes of our samples are significant higher, ranging from 2.56 $cm^3\ g^{-1}$ to 3.18 $cm^3\ g^{-1}$, in which ACB-2 shows the highest pore volume value of 3.18 $cm^3\ g^{-1}$. This can explain the highest nitrogen uptake of ACB-2 in Figure 2, since a large pore volume is beneficial to capturing nitrogen molecules. In general, it is difficult to improve the BET SSA and pore volume values simultaneously. Impressively, our samples prepared by the bead formation of the fumed silica powder possess not only high BET SSA but also high pore volume. As is seen in Table 1, BET SSA is related to the weight ratio of KOH/ACB. Hence, appropriate weight ratio of KOH/carbon beads and activation temperature are key to obtain high BET SSA and large pore volume. The average pore sizes of the samples are also listed in Table 3. As is discussed above, ACB-2 exhibits the largest pore volume, while ACB-5 possesses the largest BET SSA. Obviously, the high nitrogen adsorption amount of ACB-2 shown in Figure 2 is attributed to its meso-pores and exceptionally large pore volume, compared with the other porous carbonaceous materials.[27] Consequently, we mainly focused on two samples, ACB-2 and ACB-5 in our subsequent study. Their PSDs were calculated by the combined method of GCMC and SIE (Figure 3),[12] in which the pore size range was set to 0.5–10 nm and the pore size span in the distribution was set to 0.375 nm, which is about the size of a nitrogen molecule. We can find from Figure 3 that the pore sizes mainly center at about 3 nm with a minor part of the pores larger than 4 nm, which is in favor of CO_2 adsorption. Based on the PSD obtained, GCMC simulations for the isotherms of N_2 adsorption were carried out. Here, we assume that each pore size will contribute to the total adsorption isotherm in proportion to the fraction of the total volume of the sample. Consequently, the uptake is the sum of adsorption amounts in different sized pores, simulated by GCMC method.[12,19,28] We plotted the simulation data for N_2 adsorption obtained from the PSD along with the experimental isotherms in Figure 4, where all the simulated data coincide well with the experimental curves for the two samples. This suggests that the results of the PSD analysis are reasonable and these values can be, therefore, used in

Table 3. Parameters of the Activated Carbon Beads Measured by ASAP-2010*

Sample	S_{BET} ($m^2\ g^{-1}$)	$S_{Langmuir}$ ($m^2\ g^{-1}$)	V_t ($cm^3\ g^{-1}$)	V_{DA} ($cm^3\ g^{-1}$)	V_{meso} ($cm^3\ g^{-1}$)	Average Pore Size (nm)
ACB-1	2668	3730	2.62	0.80	1.82	3.92
ACB-2	2986	4131	3.18	0.93	2.25	4.27
ACB-3	3017	4234	3.05	0.91	2.14	4.05
ACB-4	3205	4484	2.82	0.93	1.89	2.92
ACB-5	3537	4972	2.56	1.03	1.53	2.89

*S_{BET} is the BET surface area and $S_{Langmuir}$ is the Langmuir surface area. V_t, V_{DA}, and V_{meso} are the total pore volume, micro-pore volume, and meso-pore volume, respectively.

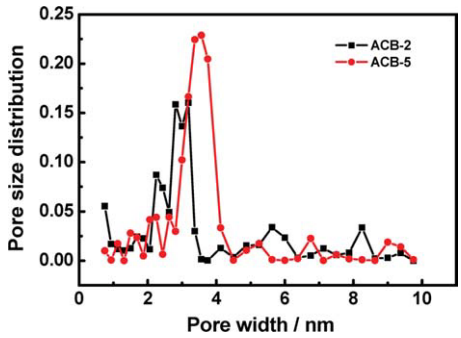

Figure 3. The pore size distribution of ACB-2 and ACB-5 calculated by using GCMC and SIE.

The solid square (in red) is for ACB-2 and the solid circle (in black) is for ACB-5 [Color figure can be viewed in the online issue, which is available at wileyonlinelibrary.com.]

our subsequent simulations for the prediction of gas adsorption of these materials.

Carbon dioxide adsorption in ACB-2 and ACB-5

The uptakes of CO_2 for ACB-2 and 5 at 298 K, 348 K, and 423 K were measured by using IGA-003 apparatus, as shown in Figure 5. It should be pointed out that to verify our results an independent measurement of the isotherm for ACB-5 was carried out in the Research and Development Center of Hiden Isochema, UK. Their data, presented also in Figure 5b, are in excellent agreement with ours. It is noticed that Furukawa et al.[9] reported a systemic survey of CO_2 adsorption. We referred to their data for CO_2 adsorption and listed them in Table 4 for comparison. It is found in Table 4 that the uptake of 909 mg g^{-1} for ACB-5 at 298 K and $P =$ 18 bar measured here is superior to all the carbonaceous materials, while it is also comparable to MOF-177 (1232 mg g^{-1} at 298 K and 20 bar) and COF-102 (1050 mg g^{-1} at 298 K and 20 bar).

As is well known, the adsorption capacity is dependent on temperature. Figure 6 shows the CO_2 uptakes in ACB-2 and ACB-5 at 298 K, 348 K, and 423 K, and 18 bar, measured in this work. The results indicate that CO_2 uptake decreases

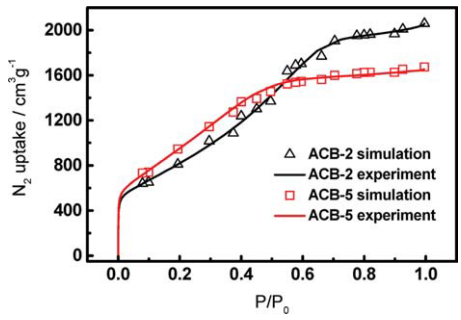

Figure 4. Comparison between experimental and simulated isotherms of nitrogen at 77 K fitted by using PSD.

The black line and red line are the experimental adsorption isotherm of ACB-2 and ACB-5, respectively. The triangle and square are the simulation adsorption isotherm of ACB-2 and ACB-5, respectively [Color figure can be viewed in the online issue, which is available at wileyonlinelibrary.com.]

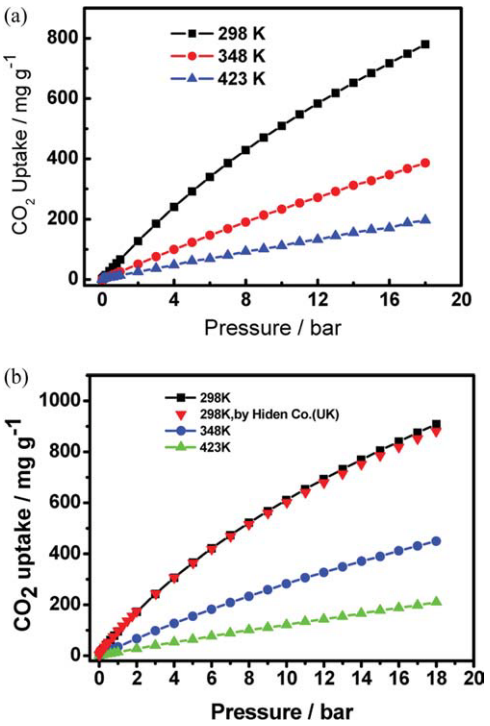

Figure 5. The experimental carbon dioxide adsorption isotherms for ACB-2 and ACB-5 at 298 K, 348 K, and 423 K, respectively.

Figure 5a presents the experimental adsorption isotherms of ACB-2 at 298 K, 348 K, and 423 K, respectively. Figure 5b presents the experimental adsorption isotherms of ACB-5 at 298 K, 348 K, and 423 K, respectively. Note that the data (down triangle) measured by Hiden Company (UK) are also shown for comparison [Color figure can be viewed in the online issue, which is available at wileyonlinelibrary.com.]

rapidly with the increase of temperature. That is to say, temperature is critical to carbon dioxide capture by adsorption.

Room-temperature methane storage in ACB-2 and ACB-5

Methane adsorption isotherms in ACB-2 and ACB-5 were also measured in this work, as shown in Figure 7. Clearly, the uptake of ACB-5 is always higher than ACB-2, although ACB-2 possesses the larger pore volume than ACB-5. The reason may be that the ACB-5 holds a larger BET SSA than ACB-2. It suggests that at middle and low pressures ($p < 18$ bar), BET SSA plays a more important role in methane adsorption, compared with pore volume. In particular, the uptake of methane in ACB-5 is 15.23 wt % at 298 K and 18 bar, which is higher than other carbonaceous materials and some other porous materials, including MOF-5[29] (10 wt % at 20 bar) and COF-102 (14 wt %, at 20 bar),[9] as shown in Table 5.

Prediction of carbon dioxide and methane at high pressure

Since our experimental measurements are limited to $P < 20$ bar for the IGA-003 apparatus, it is necessary to develop a method to predict the performances of ACB-2 and 5 at higher

Table 4. Summary and Comparison of the Uptakes of CO_2 in ACB-2, ACB-5 and in Carbon-Based Materials and Other Porous Materials in the Literature at 298 K*

Materials	S_{BET} (m^2 g^{-1})	Pore Size (nm)	Pore Volume (cm^3 g^{-1})	CO_2 Uptake (mg/g)		Refs.
				Excess	Maximum CO_2 Uptake(absolute)	
ACB-2	2986	4.27	3.18	779.9/18bar^{exp}	1421/ 60bar^{sim}	This work
ACB-5	3537	2.89	2.56	908.9/18bar^{exp}	1563/60bar^{sim}	This work
ACF	424		0.22	100.3/1bar^{exp} (293K)		4
AC	2187		1.64	484/8bar^{exp}		5
RN800(AC)	1092	1.74	0.467	96/1bar^{exp}		6
Zeolite 13X				306.24/19bar^{exp}	324.3/32bar^{exp}	7
MOF-5	3800	1.12	1.19	836/20 bar^{exp}	970/40bar^{exp}	8
MOF-177	4750	1.7		1232/20bar^{exp}	1490/40 bar^{exp}	8
COF-102	3620	1.2	1.55	1050/20bar^{exp}	1200/55bar^{exp}	9
ZIF-69	1970			13.75/1 bar^{exp}		10

pressures. As is reported in our previous work,[19,32] GCMC simulation and the PSD calculated here were used to predict adsorption of carbon dioxide and methane at higher pressures. Note that the simulated uptakes are the sum of the ones in the constituent pores described by the PSD. The simulated isotherms for CO_2 in ACB-2 and 5 are shown in Figure 8, along with the experimental data measured here. Clearly, our simulated results are in good agreement with the experimental data when $P < 18$ bar. This indicates that our GCMC simulation can be used to predictions of adsorption for ACBs at high pressures with confidence. It is found in Figure 8 that the uptakes of CO_2 increase drastically with pressure in the range of 40–60 bar. Meanwhile, the methane adsorption isotherms are given in Figure 9, in which the uptakes of CH_4 reach 18.77 wt % in ACB-2 and 21.83 wt % in ACB-5, respectively, at 298 K and 35 bar.

As is seen from Figures 8 and 9, the uptakes of both CO_2 and CH_4 increase with pressure pronouncedly. For comparison, some of the predicted uptakes of CO_2 and CH_4 at high pressures are listed in Table 4 and 5 along with the data reported in the literature. We can find from Table 4 that although the ACB-5 material exhibits CO_2 uptake of 909 mg g^{-1} at $p = 18$ bar and $T = 298$ K, it reaches 1563 mg g^{-1} at $p = 60$ bar, which is greater than maximum CO_2 uptakes of MOF-177 of 1490 mg g^{-1} at $p = 40$ bar and COF-102 of 1200 mg g^{-1} at $p = 55$ bar. We can also find from Table 5 that the maximum methane uptake of ACB-5 at $p = 35$ bar is greater than all other porous materials, including MOF-5, activated carbon and zeolite 13-X, except being slightly less than that of COF-102 of 24.3 wt % at $p = 85$ bar. It is noticeable that although all the materials mentioned above show high BET surface areas, they have different pore volumes. Obviously, the large pore volume of our samples contributes to the high CH_4 uptake at $p < 20$ bar here.

Adsorption measurement of pure N_2 and mixtures of CO_2/CH_4 and CO_2/N_2

As is mentioned in the Introduction section, separations of the mixtures of CO_2/CH_4 and CO_2/N_2 are closely related to the capture of CO_2 in the pre- and postcombustion processes. Therefore, the selectivities of ACBs in the separations are very important, which can be resolved by using experimental data and theoretical models. As for experimental measurements, in fact, only the total uptake for the gas mixture with a constant composition and the uptakes of its constituent pure components can be measured directly by the IGA-003 apparatus. As a component of the mixtures of interest in this work, the adsorption isotherms of N_2 were also measured at 298 K, 348 K, and different pressures, shown in Figure 10.

We prepared several mixture samples purposely. The compositions of the gas mixture of CO_2:CH_4 = 15:85 (mole ratio) and 30:70 are representative ones in the NG fields. On the other hand, the gas compositions of CO_2:N_2 = 20:80 (mole ratio) and CO_2:N_2 = 50:50 are selected here for the description of postcombustion flue gases. The adsorption isotherms of the mixture CO_2:CH_4 = 15:85 and 30:70 were measured on ACB-5 at 298 K, and shown in Figures 11a, b,

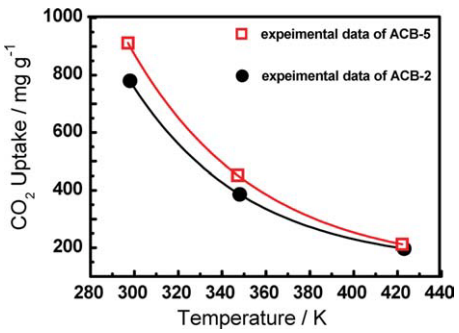

Figure 6. Carbon dioxide adsorption uptake changing with temperature.

The square and circle are the experimental data of ACB-5 and ACB-2, respectively [Color figure can be viewed in the online issue, which is available at wileyonlinelibrary.com.]

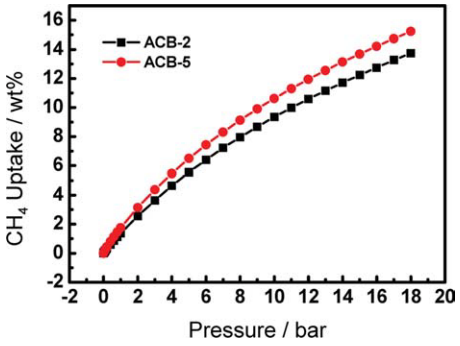

Figure 7. Experimental methane adsorption isotherms for ACB-2 and ACB-5, respectively, at 298 K, this work.

[Color figure can be viewed in the online issue, which is available at wileyonlinelibrary.com.]

Table 5. Summary and Comparison of the Uptakes of CH_4 in ACB-2, ACB-5 and in Carbon-Based Materials and Other Porous Materials in the Literature at 298 K*

Materials	S_{BET} ($m^2\ g^{-1}$)	Pore Size (nm)	Pore Volume ($cm^3\ g^{-1}$)	CH_4 Uptake (wt %)		Refs.
				Excess	Maximum CH_4 Uptake(absolute)	
ACB-2	2986	4.27	3.18	13.75/18 bar^{exp}	18.77/35 bar^{sim}	This work
ACB-5	3537	2.89	2.56	15.23/18 bar^{exp}	21.83/35 bar^{sim}	This work
ACF	2600	0.7–1.6		10.4/20 bar^{exp}	18.1/400 bar^{exp}	30
Maxtor(AC)	3250		1.79	14.4/20 bar^{exp}	19.2/50 bar^{exp}	31
MOF-5	3800	1.12	1.19	10/20 bar^{exp}	20/65 bar (300 K)^{exp}	29
COF-102	3620	1.2	1.55	14/20 bar^{exp}	24.3/85 bar^{exp}	9
Zeolite 13X				6.71/21 bar^{exp}	9.15/47 bar^{exp}	7

*The pore size and pore volume are obtained by measurements. S_{BET} is the BET specific surface area. sim means the simulation result and exp means the experimental result.

where the uptake of the mixture at CO_2:CH_4 = 15:85 rises to 19.6 wt % at 13 bar. Figure 12 presents the isotherms of the mixtures of CO_2/N_2 at different gas compositions and T = 298 K and 348 K, respectively. It is found that the adsorption amounts for the mixtures increase with pressure significantly when $P > 1$ bar. For example, for the mixture CO_2:N_2 = 50:50, the uptake of 38 wt % is reached at 13 bar and 298 K (Figure 12a), while it is 20.1 wt % for the mixture of CO_2:N_2 = 20:80 at 13 bar and 298 K (Figure 12b).

CO_2 adsorption selectivity of CO_2/CH_4 and CO_2/N_2 mixtures

To investigate the adsorption selectivity of CO_2 over CH_4 or N_2 on ACBs, the selectivity is defined by[33]

$$S_{i/j} = \frac{x_i/x_j}{y_i/y_j} \tag{3}$$

where x_i,y_i, and x_j, y_j are the mole fractions of component i and j in the adsorbed and bulk phases, respectively.

To solve the adsorption isotherms of a single component of the binary mixture for the calculation of the selectivity, many theoretical models combined with the ideal-adsorbed solution theory (IAST) have been proposed for the description of the adsorption data, such as the Langmuir model,[34] vacancy solution theory and Dual-Site Langmuir-Freundlich (DSLF).[35] The IAST was proposed by Myers and Prausnitz to predict the multi-component adsorption on the basis of the adsorption properties of pure components.[36] As described in the recent work of Babarao et al.,[35] for the storage and separation of CO_2 and CH_4 in porous materials, the IAST and DSLF combination is still a widely used model. In the IAST-DSLF model, the pure-component equilibrium data are used to correlate theoretical DSLF models, and to further predict the adsorption of each constituent component of the mixtures. The DSLF model is given by[37]

$$N^{\circ}(f) = \frac{N_1 k_1 f^{n_1}}{1 + k_1 f^{n_1}} + \frac{N_2 k_2 f^{n_2}}{1 + k_2 f^{n_2}} \tag{4}$$

where f is the fugacity of bulk gas at equilibrium with adsorbed phase, N_i, k_i and n_i are model parameters of maximum adsorption amount at site i (i = 1 or 2), the affinity constant, and the deviation from the simple Langmuir equation, respectively.

Being analogous to Raoult's law for vapor-liquid equilibrium, the IAST assumes that the adsorbed solutions are ideal and all activity coefficients in the adsorbed phase are unity. Thus, the adsorption equilibrium between adsorbed and gas phases satisfies the following equation

$$P y_i \phi_i = x_i f_i^{\circ}(\pi) \tag{5}$$

where f°_i is the fugacity of the equilibrium gas phase corresponding to the spreading pressure π for the adsorption of pure gas i, ϕ_i is the gas fugacity coefficient of component i calculated by the Peng-Robinson equation of state, and x_i and y_i are the molar fraction of component i at adsorbed and bulk phases, respectively. The binary gas mixing process is carried out at constant spreading pressure π and expressed by

$$\int_0^{f_1^{\circ}} N_1^{\circ}(f_1) d\ln f_1 = \int_0^{f_2^{\circ}} N_2^{\circ}(f_2) d\ln f_2 \tag{6}$$

where the single-component adsorption amount and selectivity are further obtained from the above equations.

From the IAST-DSLF model, the uptakes of the constituent components were solved and also shown in Figures 11 and 12, which are described by dot and dash lines.

It can be found from Figure 11 that the calculated total uptake of the mixture is in agreement with the experimental measurements. In particular, for the precombustion mixture of CO_2/CH_4 = 15:85, the calculated uptakes almost reproduce the experimental data, which indicates that the calculated selectivity is basically reasonable. When the mole ratio of CO_2 and CH_4 changes from

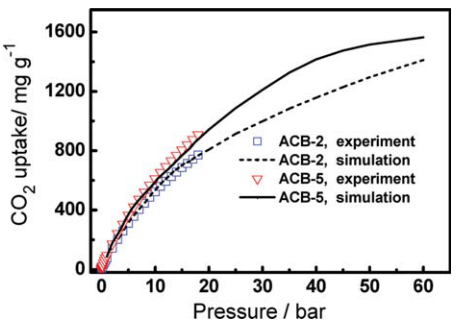

Figure 8. Simulated adsorption isotherms of CO_2 for ACB-2 and ACB-5 by using GCMC and PSD at 298 K and up to 60 bar.

For comparison, our experimental data (< 18 bar) are also shown here. The triangle and square are the experimental data of ACB-5 and ACB-2, respectively. The solid and dash lines are the simulation results of ACB-5 and ACB-2, respectively [Color figure can be viewed in the online issue, which is available at wileyonlinelibrary.com.]

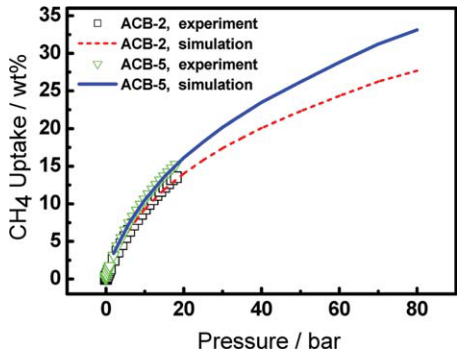

Figure 9. Simulated adsorption isotherms of CH_4 for ACB-2 and ACB-5 by using GCMC and PSD at 298 K and up to 80 bar.

For comparison, our experimental data (<18 bar) are also shown here. The solid and dash lines are the simulation results of ACB-5 and ACB-2, respectively [Color figure can be viewed in the online issue, which is available at wileyonlinelibrary.com.]

15:85 to 30:70, the selectivity of ACB for CO_2 remains in the range of 2–2.5, which is similar to the previous experimental results and the molecular simulation results.[38,39] For the postcombustion mixtures of $CO_2/N_2 = 50:50$ and 20:80, the total uptakes calculated from the IAST-DSLF model also coincide fairly with experimental measurements at different temperatures of $T = 298$ and 348 K, as shown in Figures 12a–d (solid line), which further verifies that the selectivity calculated from the IAST-DSLF model is reliable. Nevertheless, it is noticed that some deviations between the experimental and calculated results appear in Figures 11 and 12, because several assumptions are inherent in Eqs. 4–6 in the IAST-DSLF model.[36]

As is shown in Figures 11 and 12, the selectivity of ACBs for CO_2/N_2 is in the range of 6.0–8.0 at $T = 298$ K, which is about 2–3 times greater than that of CO_2 over CH_4. This observation can be attributed to the characteristics of CO_2, CH_4, and N_2 molecules. CO_2 molecules are linear ones and possess certain quadruples and therefore can be polarized rather easily. In contrast, N_2 molecules are nonpolar and smaller, compared with CH_4 molecules, as shown in Table 2. Consequently, the selectivity of ACBs for CO_2/N_2 is

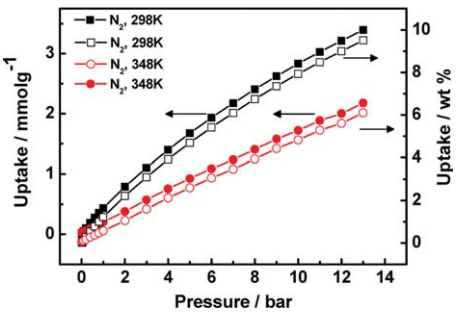

Figure 10. Experimental nitrogen adsorption isotherms at 298 K and 348 K in ACB-5.

The solid square and open square present the uptake of nitrogen at 298 K in mmol g^{-1} and wt %, respectively. The solid circle and open circle present the uptake of nitrogen at 348 K in mmol g^{-1} and wt %, respectively [Color figure can be viewed in the online issue, which is available at wileyonlinelibrary.com.]

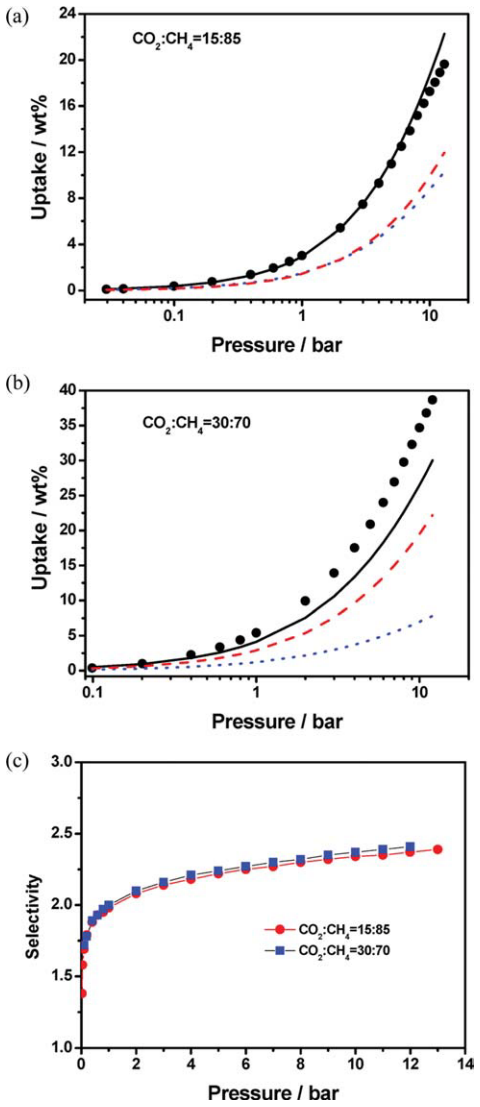

Figure 11. Experimental data and calculated isotherms in ACB-5 for the mixtures of CH_4/CO_2 at different compositions and 298 K.

The isotherms for total and the constituent components calculated from the IAST-DSLF model are also shown. The selectivity is calculated from the results of the model. (a) CO_2:CH_4:=15:85 (mole ratio), (b) CO_2:CH_4:=30:70 (mole ratio), (c) Selectivity at CO_2:CH_4 = 15:85 and 30:70 (mole ratio), ●, experimental uptake of the mixture; —, calculated uptake of the mixture; ···, calculated uptake of component CH_4; - - -, calculated uptake of component CO_2 [Color figure can be viewed in the online issue, which is available at wileyonlinelibrary.com.]

greater than CO_2/CH_4 mixture. Furthermore, with the temperature increasing to $T = 348$ K, the selectivity of ACBs for CO_2/N_2 decreases to about 4.0. Impressively, at $T = 298$ K, the selectivity of CO_2 in the mixture of $CO_2/N_2 = 50:50$ is apparently larger than that for the mixture of $CO_2/N_2 = 20:80$. In contrast, at $T = 348$ K, the selectivity of CO_2 at the two compositions are almost the same. That is to say, at $T = 298$ K, the composition of the mixture exhibits a significant effect on selectivity, while the effect becomes trivial at $T = 348$ K.

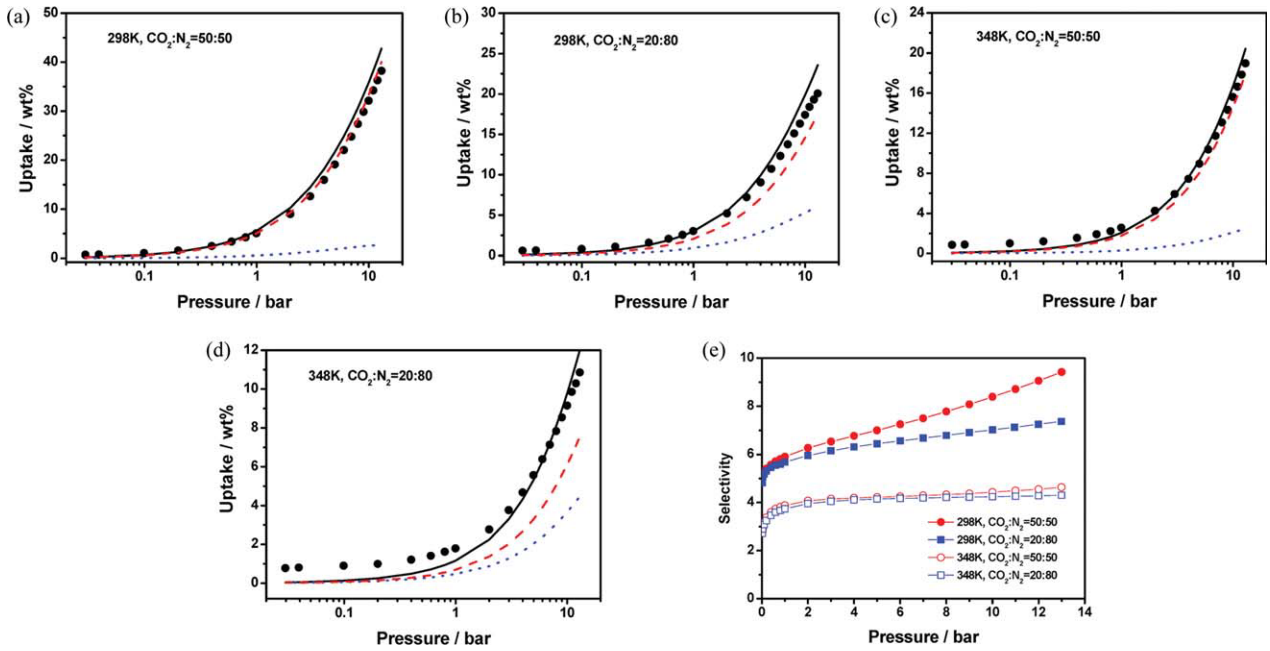

Figure 12. Experimental data and calculated isotherms in ACB-5 at 298 K for the mixtures of N_2/CO_2 at different compositions.

The isotherms for total and the constituent components calculated from the IAST-DSLF model are also shown. The selectivity is calculated from the results of the model. (a) CO_2:N_2 = 50:50 (mole ratio), 298 K, (b) CO_2:N_2=20:80 (mole ratio), 298 K, (c) CO_2:N_2 = 50:50 (mole ratio), 348 K, (d) CO_2:N_2 = 20:80 (mole ratio), 348 K, (e) Selectivity at CO_2: N_2=50:50 and 20:80 (mole ratio), T = 298 and 348 K, ●, experimental uptake of the mixture; —, calculated uptake of the mixture; ···, calculated uptake of component N_2; - - -, calculated uptake of component CO_2 [Color figure can be viewed in the online issue, which is available at wileyonlinelibrary.com.]

Conclusions

It is a challenging and urgent task to develop new porous materials for high-capacity storage of CO_2 and CH_4 by physisorption from the energy and environmental point of view. Besides, separations of the mixtures of CO_2/CH_4 and CO_2/N_2 are relevant to the important topic of pre- and postcombustion capture of CO_2. To deal with these tasks, we first prepared a series of high performance carbonaceous mesoporous materials: activated carbon beads (ACB-x, x = 1–5). Impressively, ACB-5 possesses the BET SSA of 3537 m^2 g^{-1} and ACB-2 has the pore volume of 3.18 cm^3 g^{-1}.

Experimental measurements have been carried out for the isotherms of CO_2 and CH_4. Carbon dioxide adsorption capacity of 909 mg g^{-1} has been achieved in ACB-5 at 298 K and 18 bar, which is superior to the existing carbonaceous porous materials and comparable to MOF-177 (1232 mg g^{-1} at 298 K and 20 bar) and COF-102 (1050 mg g^{-1} at 298 K and 20 bar) reported in the literature (Table 4). In addition, the methane uptake reaches 15.23 wt % in ACB-5 at 298 K and 18 bar, which is better than MOF-5 (10 wt %) and COF-102 (14 wt %) at 298 K and 20 bar (Table 5).

To predict the performances of ACB-2 and ACB-5 at high pressures, modeling of the samples and GCMC simulation have been carried out. Simulation results indicate that the uptakes of CO_2 and CH_4 may reach 1560 mg g^{-1} and 35 wt % in ACB-5 at p = 60 bar, respectively, which are among the highest capacities known.

The adsorption isotherms of CO_2/N_2 and CO_2/CH_4 in ACB-2 and ACB-5 have been measured at 298 and 348 K and different compositions. The IAST-DSLF model was used to solve the selectivity. The selectivity of ACBs for CO_2/CH_4 remains in the range of about 2–2.5 (Figure 11), while it is in the range of about 6.0–8.0 for CO_2/N_2 at T = 298 K (Figure 12), covering a certain composition range of the mixtures.

In summary, due to their thermal-stability and low cost, carbonaceous porous materials are deemed as good adsorbents in CO_2 capture. This work presents a new type of carbonaceous mesoporous materials, ACBs, which exhibit high BET SSA and exceptionally large pore volume, in particular. The adsorption isotherms of CO_2 and CH_4 and selectivity of CO_2 over N_2 and CH_4 show that the ACBs prepared here are not only good candidates for CO_2 and CH_4 storage, but also for the capture of carbon dioxide in pre- and postcombustion processes.

Acknowledgments

This work was supported by NSF of China (20736002), National Basic Research Program of China (2011CB706900), National Scientific Research Funding (ZD0901) and Chemical Grid Program from BUCT. We are also grateful to Dr. D. Broom of Hiden Isochema Ltd, UK, for his measurements of the uptakes of CO_2 in one of our samples for data verification.

Literature Cited

1. Morris RE, Wheatley PS. Gas storage in nanoporous materials. *Angew Chem Int Ed Engl*. 2008;47:4966–4981.
2. Xiang ZH, Cao DP, Lan JH, Wang WC, Broom D. Multiscale simulation and modeling of adsorptive processes for energy gas storage and CO_2 capture in porous coordination frameworks. *Energy Environ Sci*. 2010;33:1469–1487.
3. Peng X, Zhao J, Cao DP. Adsorption of carbon dioxide of 1-site and 3-site models in pillared clays: a Gibbs ensemble Monte Carlo simulation. *J Colloid Int Sci*. 2007;310:391–401.

4. An H, Feng B, Su S. CO_2 capture capacities of activated carbon fibre-phenolic resin composites. *Carbon*. 2009;47:2396–2405.
5. Pellerano M, Pre P, Kacem M, Delebarre A. CO_2 capture by adsorption on activated carbons using pressure modulation. *Energy Procedia*. 2009;1:647–653.
6. Pevida C, Plaza MG, Arias B, Fermoso J, Rubiera F, Pis J. Surface modification of activated carbons for CO_2 capture. *J Appl Surf Sci*. 2008;254:7165–7172.
7. Cavenati S, Grande CA, Rodrigues AE. Adsorption equilibrium of methane, carbon dioxide, and nitrogen on zeolite 13X at high pressures. *J Chem Eng Data*. 2004;49:1095–1101.
8. Millward AR, Yaghi OM. Metal-organic frameworks with exceptionally high capacity for storage of carbon dioxide at room temperature. *J Am Chem Soc*. 2005;127:17998–17999.
9. Furukawa H, Yaghi OM. Storage of hydrogen, methane, and carbon dioxide in highly porous covalent organic frameworks for clean energy applications. *J Am Chem Soc*. 2009;131:8875–8883.
10. Banerjee R, Phan A, Wang B, Knobler C, Furukawa H, O'Keeffe M, Yaghi OM. High-throughput synthesis of zeolitic imidazolate frameworks and application to CO2 capture. *Science*. 2008;319:939–943.
11. Alcaniz-Monge J, DelaCasa-Lillo MA, Cazorla-Amoros D, Linares-Solano A. Methane storage in activated carbon fibres. *Carbon*. 1997;35:291–297.
12. Shao XH, Wang WX, Xue RS, Shen ZM. Adsorption of methane and hydrogen on mesocarbon microbeads by experiment and molecular simulation. *J Phys Chem B*. 2004;108:2970–2978.
13. Cao DP, Zhang XR, Chen JF, Wang WC, Yun J. Optimization of single-walled carbon nanotube arrays for methane storage at room temperature. *J Phys Chem B*. 2003;107:13286–13292.
14. Esteves I, Lopes MS, Nunes PM, Mota JPB. Adsorption of natural gas and biogas components on activated carbon. *Sep Purif Technol*. 2008;62:281–296.
15. Li LX, Song H, Chen X. Ordered mesoporous carbons from the carbonization of sulfuric-acid-treated silica/triblock copolymer/sucrose composites. *Micropor Mesopor Mater*. 2006;94:9–14.
16. Qian XF, Wan Y, Wen YL, Jia NQ, Li HX, Zhao DY. Synthesis of ordered mesoporous crystalline carbon-anatase composites with high titania contents. *J Colloid Int Sci*. 2008;328:367–373.
17. Carcia-Blanco AA, de Oliveira JCA, Lopez R, Moreno-Pirajan JC, Giraldo L, Zgrablich G, Sapag K. A study of the pore size distribution for activated carbon monoliths and their relationship with the storage of methane and hydrogen. *Colloids Surf. A: Physicochem. Eng. Aspects*. 2010;357:74–83.
18. Perez-Mendoza M, Schumacher C, Suarez-Garcia F, Almazan-Almazan MC, Domingo-Garcia M, Lopez-Garzon FJ, Seaton NA. Analysis of the microporous texture of a glassy carbon by adsorption measurements and Monte Carlo simulation. Evolution with chemical and physical activation. *Carbon*. 2006;44:638–645.
19. Cao DP, Wang WC, Shen ZG, Chen JF. Determination of pore size distribution and adsorption of methane and CCl4 on activated carbon by molecular simulation. *Carbon*. 2002;40:2359–2365.
20. Stubbs JM, Wilhem DD, Siepmann JI. Partial molar volume and solvation structure of naphthalene in supercritical carbon dioxide: a Monte Carlo simulation study. *J Phys Chem B*. 2005;109:19885–19892.
21. Murthy CS, Singer K, Klein ML, McDonald IR. Pairwise additive effective potentials for nitrogen. *Mol Phys*. 1980;41:1387–1399.
22. Jiang SY, Rhykerd CL, Gubbins KE. Layering, freezing transitions, capillary condensation and diffusion of methane in slit carbon pores. *Mol Phys*. 1993;79:373–391.
23. Cao DP, Shen ZG, Chen JF, Zhang XR. Experiment, molecular simulation and density functional theory of the fluid confined in MCM-41. *Micropor Mesopor Mater*. 2004;67:159–166.
24. Steele WA. The physical interaction of gases with crystalline solids: I. gas-solid energies and properties of isolated adsorbed atoms. *Solids Surf Sci*. 1973;36:317–352.
25. Liu H, Xue RS, Yu JM, Shen ZM. Influences of adding silica on structure and capacitive performance of activated carbon. *Chin J Power Sources*. 2009;33:204–212.
26. Wang HL, Gao QM, Hu J. High hydrogen storage capacity of porous carbons prepared by using activated carbon. *J Am Chem Soc*. 2009;131:7016–7022.
27. Shen CZ, Grande CA, LI P, Yu JG, Rodrigues AE. Adsorption equilibria and kinetics of CO2 and N2 on activated carbon beads. *Chem Eng J*. 2010;160:398–407.
28. Neimark AV, Ravikovitch PI. Capillary condensation in MMS and pore structure characterization. *Micropor Mesopor Mater*. 2001;44–45:697–707.
29. Zhou W, Wu H, Hartman MR, Yildirim T. Hydrogen and methane adsorption in metal organic frameworks: a high pressure volumetric study. *J Phys Chem C*. 2007;111:16131–16137.
30. Lm JS, Jung MJ, Lee YS. Effects of fluorination modification on pore size controlled electrospun activated carbon fibers for high capacity methane storage. *J Colloid Interface Sci*. 2009;339:31–35.
31. Himeno S, Komatsu T, Fujita S. High-pressure adsorption equilibria of methane and carbon dioxide on several activated carbons. *J Chem Eng Data*. 2005;50:369–376.
32. Shao X, Wang WC, Zhang XJ. Experimental measurements and computer simulation of methane adsorption on activated carbon fibers. *Carbon*. 2007;45:188–195.
33. Cao DP, Wu JZ. Modeling selectivity of activated carbons for efficient separation of hydrogen and carbon dioxide. *Carbon*. 2005;43: 1364–1370.
34. Markham ED, Benton AF. The adsorption of gas mixtures by silica. *J Am Chem Soc*. 1931;53:497–506.
35. Babarao R, Hu ZQ, Jiang JW, Chempath S, Sandler SI. Storage and separation of CO2 and CH4 in silicalite, C168 schwarzite, and IRMOF-1: a comparative study from Monte Carlo simulation. *Langmuir*. 2007;23:659–666.
36. Myers AL, Prausnitz JM. Thermodynamics of mixed-gas adsorption. *AIChE J*. 1965;11:121–127.
37. Ruthven DM. *Principles of Adsorption and Adsorption Processes*. New York: Wiley, 1984.
38. Kurniawan Y, Bhatia SK, Rudolph V. Simulation of binary mixture adsorption of methane and CO_2 at supercritical conditions in carbons. *AIChE J*. 2006;52:957–967.
39. Peng X, Wang WC, Xue RS, Shen Z. Adsorption separation of CH_4/CO_2 on mesocarbon microbeads: experiment and modeling. *AIChE J*. 2006;52:994–1003.

Manuscript received Jun 15, 2010, and revision received Nov. 2, 2010.